POLITECNICO DI TORINO
Repository ISTITUZIONALE

Potential of multiple injection strategies implementing the after shot and optimized with the design of experiments procedure to improve diesel engine emissions and performance

(Article begins on next page)

18 May 2024

1   **POTENTIAL OF MULTIPLE INJECTION STRATEGIES IMPLEMENTING THE AFTER SHOT**

2   **AND OPTIMIZED WITH THE DESIGN OF EXPERIMENTS PROCEDURE TO IMPROVE**

3   **DIESEL ENGINE EMISSIONS AND PERFORMANCE.**

4   *d'Ambrosio, S. , and Ferrari, A.*[*]

5   *Energy Department – Politecnico di Torino*

6   *C.so duca degli Abruzzi, 24, 10129, Torino, Italy.*

7   **1.   ABSTRACT.**

8   The potential of the after-injection versus engine-out emissions, combustion noise and brake specific fuel consumption

9   has been evaluated for a Euro 5 diesel engine with a reduced compression ratio (16.3:1). The engine has been fueled

10 with conventional diesel fuel. In particular, the effects of injection strategies that feature either pilot and after-injection

11 shots, or double-pilot and single-after injection shots, have been assessed experimentally, in the presence of high *EGR*

12 fractions. Calibrations with triple and quadruple injection schedules have been optimized by means of a design of

13 experiments procedure. The performance of the thus calibrated propulsion system has been compared with data from a

14 previously optimized double injection schedule, characterized by a retarded main injection timing in order to intensify

15 the premixed combustion. The experimental data refer to different steady-state working conditions that are

16 representative of passenger car engine applications over the European homologation cycle. In-cylinder analyses of the

17 pressure, heat release rate, temperature and emissions have been performed in order to have a better understanding of

18 the effects of the implemented injection strategies on engine performance.

19 The substitution of the pilot- main injection schedule in the higher part-load zone of the *NEDC* region with a triple

20 injection, featuring both pilot and after shots, has led to lower NO_x and higher soot, while fuel consumption remains

21 almost the same. In general, the *EGR* trade-off soot-NO_x, *bsfc*-NO_x, *HC*-NO_x and *CO*-NO_x curves do not change to any

22 significant extent when an after shot is added to the pilot-main injection train. Reductions in the combustion noise,

23 which depend on the changes in the pilot injection parameters that result from the design of experiments procedure, can

24 also be obtained, as a consequence of the addition of the after-injection to the pilot-main injection schedule. Pilot-pilot-

25 main-after strategies guarantee improved NO_x-soot and *bsfc*-NO_x *EGR* trade-off curves at medium to high loads and at

---

[*] Corresponding author e-mail address: alessandro.ferrari@polito.it.

26 low to medium speeds, compared to both pilot-pilot-main and pilot-main-after strategies, and allow combustion noise to

27 be diminished significantly.

28 **Keywords**: after injection; design of experiments; partial premixed charge compression ignition engines.

29 **Highlights:**

30 - The benefits of after injections are evaluated in a low-compression ratio Euro 5 diesel engine.

31 - Triple and quadruple injection schedules are compared with pilot-main and pilot-pilot-main strategies.

32 - The potential of after injections is examined in the higher part of the *NEDC* load zone.

33 **2. INTRODUCTION**

34 The fuel injection strategy can play an important role in simultaneously reducing passenger car diesel engine emissions

35 [1, 2, 3, 4] and combustion noise [5], without neglecting fuel consumption targets. In other words, a multiple injection

36 strategy, adopted to replace a single fuel injection shot with multiple discrete fuel injection events of reduced size, can

37 easily be implemented using Common Rail (*CR*) systems, equipped with the modern injectors [6, 7]. These injectors

38 can control small injected fuel quantities, despite pressure waves, and guarantee superior flexibility in the management

39 of the dwell time, in order to fulfil Euro 5 and Euro 6 standards.

40 There are two primary multiple injection modes: the first elemental mode, which uses pilot injection, can be

41 implemented by injecting an amount of fuel prior to the main injection (the pilot injected mass is small in conventional

42 diesel combustion systems, but can also be significant in low temperature combustion strategies [2]), while the other

43 employs after-injection, which consists of a small amount of fuel being injected separately, at the end of the main

44 injection. The benefits and effects of pilot injections on emissions, combustion noise (*CN*) and fuel consumption have

45 been evaluated and discussed in [8]. The focus of this work is on the exploitation of optimized after-injection in

46 multiple injection strategies, in order to improve engine out emissions and in-cylinder performance. From this point of

47 view, after-injection is efficient in reducing the soot engine-out emissions [9], which can be up to 40% lower than in the

48 single injection case [10]. In general, after-injections can oxide part of the unburned fuel and a decrease in *CO*, *HC* and

49 *PM* engine-out emissions is obtained [11]. The benefits increase when mixing is difficult, i.e. at medium to high loads

50 and under high *EGR* conditions when the utilization of in-cylinder air is critical [12, 13].

51 After-injections have also been proposed as a means of reducing turbocharger lag during engine transients, since the

52 pressure and the temperature of the exhaust gas leaving the cylinder can be raised significantly [14]. This makes the

53 turbocharger accelerate more quickly and allows the aggressive increase in the injection quantity to be started sooner,

54 since the fuel quantity growth must follow the increase in the air supply in order to avoid high soot during transients.

55 Finally, after-injections can be applied to raise the diesel oxygen catalyst (*DOC*) temperature above its light-off

56 temperature after a cold start and post injections[1] can then be supplied to raise the exhaust temperature even further [15,

57 16].

58 Soot emissions are affected remarkably by the duration of the main injection. In fact, an important source of smoke

59 emissions exists in diesel engines at the end of main combustion, because both the equivalence ratio and local in-

60 cylinder temperature are high [17]. In particular, when long main-injection durations are considered, even a small

61 reduction in the energizing time of the main injection can provide significant soot benefits [18]. The shortened temporal

62 length of the main injection in multiple injection schedules featuring an after shot, produces less soot. Furthermore, the

63 contribution of soot from after-injected fuel, if planned correctly, can be lower than in the case in which the after-

64 injected fuel is included in the main injection [19]. When after-injection fuel is introduced into the combustion chamber,

65 the local equivalence ratio is lower than it is at the end of the main injection without after-injection. In fact, the fuel is

66 not injected at the same location since the piston is moving [20]. An enhanced air-fuel mixing occurs, due to the

67 presence of two separate smaller combustion events [10], according to a split flame type behaviour [17]. Furthermore,

68 improved particulate oxidation occurs later on in the combustion cycle, because of the increased in-cylinder bulk

69 temperatures during the expansion stroke [21].

70 An optimum main-after *DT* value, which depends on the after injected mass, exists for the optimization of the

71 interaction between the combustion of the main injection and the combustion of the after injection, as well as for the

72 subsequent minimization of the soot produced in the overall combustion [22]. In fact, if the *DT* is too short, the after

73 fuel is injected into the regions where the combustion of the main fuel takes place. The atomized fuel spray lacks

74 oxygen because the after-injection entrains the burned gases. As a result, combustion progresses gradually, causing a

75 low heat release peak and the slow combustion rate during diffusion combustion causes the smoke emissions to

76 increase. In these cases, the after-injection produces additional soot rather than oxidizing the previously formed soot, as

77 a consequence of the main injection. On the other hand, if the after pulse is too late, the combustion of the after fuel

78 occurs at excessively reduced temperatures and, although the soot production, which is due to the after injected fuel is

79 limited (this production becomes virtually null for an after injection into surrounding gases with lower temperatures

80 than 700 K [23]), the after-shot is once again unable to properly oxidize the soot produced during the main combustion.

81 The greatest smoke reduction is achieved when the start of the after-injection is phased within a tiny window of the

82 main diffusive flame [20] in order to guide the after-fuel into the squish volume [24]. The optimum *DT* value is in the

83 600÷1000 μs range for passenger cars (instead the optimum after injection timing is in the 30-40° *CA ATDC* for delayed

84 main injection timings in heavy duty engines [25, 24]) and a constant *DT*, which corresponds to the optimum value, is

85 usually applied in the *ECU* maps for a medium speed and load range. As the mass of the after-injected fuel increases,

86 the main-after DT that minimizes the soot emissions, tends to augment. The quantity of the after injection is also a

87 trade-off: if this quantity is too small, there is no significant effect of the after-shot and, if the fuel quantity is too high,

88 the higher fuel mass has to burn in a high equivalence ratio environment [20]. The optimum after injection quantity is in

89 the 1.5÷3 mm³ range (around 15-20% of the total fuel mass in heavy duty engines [24]), i.e. small enough to prevent a

90 quasi-steady diffusion flame from being established [23].

91 Main-after injection strategies also affect NO_x, $bsfc$ and CO engine-out emissions. The presence of an after injection can

92 make the last part of the HRR curve of a pilot-main combustion rise faster than in the case without an after-injection,

93 even though all the fuel is introduced earlier in the latter case [17]. The smaller the size of the after injection, the higher

94 the acceleration of the final stage of combustion. Therefore, if a small after-injection is placed close to the main

95 injection, the combustion process can conclude earlier than in the without the after-shot case. This can explain why the

96 engine efficiency can be higher and the engine exhaust temperature can be lower when an early after-injection is used

97 [26]. If the after-injection is phased close to the main injection, the combustion barycentre moves toward the TDC and

98 the flame temperatures rise, thus leading to higher level of NO_x emissions and lower CO emissions than in the absence

99 of the after shot. If the after-injection timing occurs sufficiently far from the main injection, the NO_x emissions improve

100 compared to the without the after-injection case, whereas the fuel economy undergoes penalties for larger after

101 injections, which lead to higher $bsfc$ reductions. Finally, the after-injection spray, for after injection timings at about 40°

102 $CA\ ATDC$, reaches the wall of the liner, creating wall-wetting and thus rapidly increasing HC and $bsfc$ [27].

103 When heavy EGR rates (EGR fractions around 60%) are applied to control NO_x, most of the after injection cases

104 generate an increment in the soot and in HC and CO, because the after injected fuel cannot burn well due to the poor

105 oxygen concentration and delayed ignition [28]. This effect is in contrast with the main effect of after injection under

106 moderate EGR rates (EGR fractions in the 25÷40 range). However, a small amount of fuel, injected in an after-injection

107 with a short dwell time with respect to the main injection, can reduce fuel consumption, soot, HC and CO, compared to

108 single injections, even for heavy EGR rates [29].

109 An after-injection can be effectively combined with one or more pilot shots in order to develop sophisticated injection

110 strategies for the control of engine-out emissions, combustion noise and fuel consumption, in the medium load and

111 speed area of a low-compression ratio engine. Contributions on this topic are available in the literature [27, 30, 31], but

112 lack of information is still present about the impact of optimized calibrations featuring the after injection.

113 In the present work, the potentialities of triple and quadruple injection schedules are evaluated and the results on

114 emissions and performance, in the presence of an after-shot, are compared with those referring to pilot-main and pilot-

115 pilot-main injection strategies, at different steady-state engine working conditions. All the triple and quadruple injection

116 engine calibrations have been optimized with the design of experiment (DoE) technique, and the pilot-main injection

117   engine calibration represented a state-of-the-art double injection calibration. This comparison between optimum

118   calibrations therefore allows the effective benefits of the after injection to be assessed. Furthermore, the after injection

119   is implemented in the presence of high *EGR* rates, whereas most of the researches on the after shot are conducted under

120   low or moderate *EGR* conditions [32].

121   **3.**   **EXPERIMENTAL SETUP AND ADOPTED INEJCTION STRATEGIES.**

122   The experimental tests have been carried out on the highly-dynamic test bench, installed at the Politecnico di Torino

123   ICEAL (IC Engines Advanced Laboratory) and equipped with an 'ELIN AVL APA 100' cradle-mounted AC

124   dynamometer. An 'AVL KMA 4000' has been used to continuously meter fuel consumption, with a reading accuracy of

125   0.1% over a 0.28-110 kg/h range. Furthermore, an 'AVL AMAi60' system, made up of different analyzer trains, has

126   been applied to measure the engine-out gaseous raw emissions of *HC*, NO_x and *CO*, as well as the CO_2 levels in the

127   intake manifold, in order to evaluate the *EGR* rate. Finally, an AVL 415S smokemeter allows the engine-out soot

128   emissions to be evaluated in the exhaust gases.

129   The experimental data have been analyzed with the support of a previously developed three-zone combustion model

130   [33]. Ordinary differential mass and energy conservation equations have been applied to the fuel, unburned gas and

131   burned gas zones and have been solved numerically, on the basis of the experimental in-cylinder pressure. The model

132   allows the temperatures of the three zones to be predicted as functions of the crank angle. Furthermore, thermal and

133   prompt *NO* mechanisms are implemented in the code, according to the Zeldovich and Fenimore submodels,

134   respectively. The soot formation is modeled [42] by means of an expression that considers the mean air-fuel ratio over

135   the combustion period, while the soot oxidation rate is modeled using an empirical law, based on the temperature of the

136   burned gas zone.

137   Table 1 reports the scheme and the main features of the investigated Euro 5 passenger car diesel engine, fueled with

138   conventional diesel oil. This engine has been equipped with a *DOC* and a diesel particulate filter, while no

139   aftertreatment device has been designed to reduce the NO_x emissions. The engine has been fully instrumented with

140   piezoresistive pressure transducers and thermocouples, in order to measure the pressure and temperature in the intake,

141   exhaust and *EGR* lines of the engine. A high-frequency piezoelectric transducer has been installed in the glow-plug seat

142   to measure the pressure time-histories of the gases in the combustion chamber of one cylinder. Another piezoresistive

143   transducer has been used to detect the pressure levels in the inlet runner of the same cylinder and thus to reference the

144   in-cylinder pressure.

145   The implemented triple (both pilot-pilot-main and pilot-main-after) and quadruple (pilot-pilot-main-after) engine

146   calibrations have been optimized by means of the design of the experiments (*DoE*) statistical technique [8]. The

147 following parameters were considered as the most relevant input variables for the procedure: rail pressure (p_{Rail}), swirl

148 actuator position (Sw), dwell times between consecutive injections (DT_{Pil1} between the pilot 1 and main shots, DT_{Aft}

149 between the main and after shots and DT_{Pil2} between the pilot 2 and pilot 1 shots in quadruple injection strategies, where

150 pilot 1 is the closest shot to the main injection and pilot 2 the furthest shot from the main injection), main injection

151 timing (SOI_{Main}), the injection quantities in each pilot or after shot (q_{Pil1}, q_{Aft} and q_{Pil2} in quadruple injection strategies),

152 the inducted air per stroke and per cylinder (m_a) and the boost pressure (p_{Boost}) at high load.

153 An engine working-point, evaluated as representative of engine application to a passenger car over the new European

154 driving cycle, has been considered a key point. The following key-points were selected for the considered engine (n

155 [rpm]$\times bmep$ [bar]): 1500$\times$2, 1500$\times$5, 2000$\times$2, 2000$\times$5, 2500$\times$8, 2750$\times$12 and idle.

156 For instance, Tables 2-4 report (second column) the parameter levels that were considered in the variation lists for the

157 optimizations of the pMa injection schedule, at the 2000$\times$5 and 2750$\times$12 key-points, and of the $ppMa$ strategy, at the

158 1500x5 key-point. The center and the extreme values of the levels that were considered for each parameter were chosen

159 on the basis of preliminary measurements. An appropriate number of levels was selected in order to obtain accurate

160 results with a reasonable number of tests for each variation list. The quantity of fuel in the main injection is set by the

161 test-bench control system, in order to guarantee the $bmep$ value, and is therefore not present as a parameter in the

162 variation list. The inducted air (m_a), measured by means of the air mass flowmeter, was considered in the variation lists,

163 instead of the EGR ratio. The p_{Boost} pressure only appears in the variation list of 2750x12 since has a lower influence for

164 the other key points, which Tables 2 and 4 refer to. Furthermore, the simultaneous control of p_{Boost} and EGR can

165 constitute a problem in the presence of high X_{EGR} values, which occur at key points 2000x5 and 2750x12.

166 The preliminary variation list of each considered key-point was obtained using the Matlab Model-Based Calibration

167 toolbox, setting a V-optimal type design of experiments, which minimizes the prediction error variance, and a full

168 factorial series, as the candidate set, on the basis of the levels shown in Tables 2-4. The final variation lists were made

169 up of 120-150 tests for each considered key point, including replications of the central point (defined by the center

170 value of the levels for each parameter).

171 Once the variation list tests had been carried out, on the engine, it was possible to obtain quadratic models of the output

172 variables as functions of the input variables and of their interactions. The engine-out specific NO_x, CO, HC and soot

173 emissions, the $bsfc$ and the CN were considered as the output variables. Different targets can be introduced for the

174 output variables in order to select the best set of values for the input variables at each key point, that is, the optimized

175 engine calibration. In the present work, the optimization strategy for the triple and quadruple injection calibrations,

176 based on the DoE, has been aimed at minimizing the NO_x emissions and at reducing the combustion noise, compared to

177 the pilot-main injection baseline calibration, which was originally implemented in the ECU provided by the engine

178   *OEM*. In fact, the goal is to avoid the application of any aftertreatment device for the NO_x emissions. The presence of a

179   *bsfc-NO_x* trade-off constituted a constrain to the simultaneous reduction in *bsfc* and NO_x and a slight increase in *bsfc* has therefore

180   been accepted

181   Tables 5-7 show the reference values of the output variables for the pilot-main injection strategy and the constraints

182   used for the optimization of the triple and quadruple injection strategies, which Tables 2-4 refer to. The optimized

183   values of the input variables, calculated by means of the DoE procedure, are reported in the third column of Tables 2-4.

184   *EGR* trade-offs have been performed in the neighborhood of the baseline calibration points for the double, triple and

185   quadruple injection strategies, in order to compare not only the baseline points of the different calibrations, but the

186   complete EGR curves. The considered engine calibrations are characterized by elevated *EGR* mass fractions (

187    $X_{EGR} = \dot{m}_{EGR}/(\dot{m}_a + \dot{m}_{EGR})$)), within the 45-55% range.

4   PILOT-MAIN-AFTER INJECTION STRATEGIES.

189   If reference is made to the pilot-main (*pM*) and pilot-main-after (*pMa*) baseline calibrations at *bmep*=5 bar and *n*=2000

190   rpm, the addition of an after injection, featuring a relatively late timing (SOI_{after}≈20° *CA ATDC*) with respect to the

191   main injection, leads to a significant reduction in the NO_x emissions (cf. Fig. 1, the contoured triangle and circle

192   symbols) and in *CN* (cf. Fig. 2, the contoured triangle and circle symbols), while *bsfc*, soot, *HC*, and *CO* (cf. Figs. 3-6,

193   the contoured triangle and circle symbols) become worse. However, the penalties on soot, *HC* and *CO* are acceptable,

194   since the engine is equipped with both a *DOC* and a particulate filter. In general, *CN* improves by about 1.2÷1.5 dB for

195   the different X_{EGR} values in the *pMa* case (Fig. 2), while the *bsfc-NO_x*, soot-NO_x, *HC-NO_x* and *CO-NO_x* *EGR* trade-off

196   curves (Figs. 3-6) coincide for the *pM* and the *pMa* strategies.

197   Figures 7-10 compare the crankshaft angle based distributions of the *HRR*, T_b, NO_x and soot for the baseline calibrations

198   of the *pM* and the *pMa* strategies (as previously mentioned, the *pMa* baseline calibration is the output of the *DoE*

199   optimization procedure). Since the timing adopted for the after-injection is delayed, the after combustion (Fig. 7) takes

200   place under low in-cylinder pressure and gas temperatures (Fig. 8), and the peak burned gas temperature also reduces

201   for the *pMa* strategy, due to the higher X_{EGR} value. Furthermore, the residence time of the burned gases at higher

202   temperatures than 1950 K is longer for the *pM* calibration (Fig. 8). Finally, the proximity of the pilot combustion to the

203   main combustion and the increased X_{EGR} value can lead to richer stoichiometric equivalence ratios for the *pMa* strategy

204   at the start of the main combustion. All of these circumstances induce increased NO_x emissions for the *pM* strategy,

205   compared to the without after-injection case (Fig. 9), because the thermal NO_x increase with the value of the flame

206   temperature during the diffusive portion of combustion and are only produced in the presence of sufficient O_2

207   concentrations in the post-flame zones [34]. The reduced *DT* between the pilot and main injection in the *pMa* strategy

208   allows a softer transition between the pilot and main combustion (the *HRR* peak of the main combustion is higher for

209   the *pM* case), and is therefore beneficial in suppressing combustion noise.

210   As far as the *PM* is concerned (Fig. 10), the low-temperature combustion of the after-injected fuel does not generally

211   oxidize the previously formed soot. Furthermore, the presence of heavy *EGR* rates prevents the after-injected fuel from

212   burning well, because of a lack of oxygen concentration. As a consequence, the after injection on its own produces

213   increments in the quantity of the particulate matter, and this is proved by the change in rate, which occurs at $\theta \approx 385°$ *CA*

214   along the soot curve of the *pMa* strategy. The higher soot level obtained for the *pMa* strategy is also the result of the

215   lower premixed portion of its main combustion: in fact, the *HRR* peak pertaining to the main combustion in Fig. 7 is

216   higher for the *pM* strategy than for the *pMa* one.

217   As already mentioned, the *pMa* calibration selected in the present case has had the aim of reducing the NO_x emissions

218   and combustion noise [35]; the soot emissions are controlled by the retarded SOI_{Main} ($\approx 2°$ *CA ATDC*) and, above all, by

219   the diesel particulate filter (cf. also Table 5).

220   The *HC* and *CO* emissions in Figs. 5 and 6 are higher for the *pMa* baseline calibration point because of the retarded

221   after combustion [36, 10], which causes incomplete oxidation, and because of the possible presence of a greater number

222   of over-rich mixture zones at the start of combustion of the main injected fuel (cf. also Table 5).

223   Finally, the delayed after-injection (cf. *MFB50* values in Fig. 11) raises the temperature at the engine exhaust (cf. T_{exh} in

224   Fig. 12) for the *pMa* baseline calibration. This leads to a larger thermal energy loss at the engine exhaust and thus

225   explains the slight deterioration in the *bsfc*, shown in Fig. 3, and also found in [37]. On the other hand, the higher T_{exh}

226   values can be exploited to reduce the turbocharger lag during engine transients.

227   Figures 13-20 refer to n=2500 rpm and *bmep*=8 bar. The main difference in the *HRR* diagrams in Fig. 13, compared to

228   those in Fig. 7, concerns the position of the pilot injection, which occurs earlier for the *pMa* strategy. Furthermore, the

229   rail pressure level is $p_{rail} \approx 1200$ bar at this key-point for the *pM* calibration, whereas it reduces to $p_{rail} \approx 1125$ bar for the

230   *pMa* calibration (a higher injection pressure promote a better air-fuel mixing [38]). No pilot combustion occurs in the

231   *pMa* case, and the role of the main injection is therefore to trigger fuel ignition, which can cause interference between

232   the pilot injected fuel flames and the main injection (the soot increases significantly in Fig. 17 for the *pMa* case).

233   The NO_x and *CN* are lower for the baseline point of the *pMa* calibration (cf. Fig. 20), and the causes of the improved

234   NO_x are again the decreased residence time of the burned gas at very high temperatures, the reduced p_{nom} value and the

235   relatively high local equivalence ratios in the $360°$ *CA* $<\theta<390°$ *CA* range (cf. Figs 14 and 15). The soot and *CO*

236   emissions are better for the *pM* injection baseline calibration (cf. Figs. 17 and 19) and the reasons for this are the same

237   as those provided for the previously analyzed engine key-point. However, unlike for n=2000 rpm and *bmep*=5 bar, the

238   soot-NO_x and CO-NO_x trade-offs become slightly worse for the *pMa* strategy, and the CN-NO_x curve of the *pMa*

239   strategy is no better than that of the *pM* strategy. The general improvement in the *HC* emissions that results from the

240   application of the *pMa* injection schedule (cf. Fig. 18) is related more to the absence of the pilot combustion (the main

241   injection triggers the ignition of the pilot injected fuel for the *pMa* strategy and this probably reduces the occurrence of

242   overleaning) or to the reduced rail pressure level than to the addition of the after shot.

243   The *bsfc-NO$_x$* trade-off, the soot-*NO$_x$* trade-off, the *CO-NO$_x$* trade-off and the *CN-NO$_x$ EGR* curve for *n*=2750 rpm and

244   *bmep*=12 bar are reported in Figs. 21-24. The *pMa* calibration improves the soot-*NO$_x$* and the *CO-NO$_x$* trade-offs, but

245   penalties are incurred in *bsfc* (cf. also Table 6). The *HC-NO$_x$* trade-off also improves for the *pMa*, but the *HC* values are

246   lower than 0.1 g/kWh for both strategies and are therefore not a cause of concern. The *CO* emission levels in Fig. 23 are

247   not critical either.

248   **5   PILOT-PILOT-MAIN-AFTER INJECTION STRATEGIES.**

249   Double *pM* and triple *ppM* injection strategies have been compared with *pMa* and *ppMa* strategies at medium load and

250   speed conditions.

251   Figures 25-29 report the experimental results at *bmep*=5 bar and *n*=1500 rpm for the different calibrations. The triple

252   injections (either *ppM* or *pMa*) do not improve the *bsfc-NO$_x$* (Fig. 25), soot-*NO$_x$* (Fig. 26) *HC-NO$_x$* (Fig. 27) or *CO-NO$_X$*

253   (Fig. 28) *EGR* trade-offs, compared to the *pM* calibration. The *CN-NO$_x$* curve (cf. Fig. 29) does not change either when

254   passing from the *pM* to the *ppM* or *pMa* injection schedules.

255   No discrepancy can be observed between the results concerning *CN* in Fig. 29 and those reported in Figs. 2, which refer

256   to a similar working condition. In fact, the higher the engine speed at fixed *bmep*, the higher the combustion noise levels

257   [39]. Furthermore, Fig. 30 shows that the pilot and main combustion events are clearly distinct for both the *pM* and the

258   *pMa* baseline calibration points, unlike the events shown in Fig. 7, where the transition from the pilot to the main

259   combustion was softer for the *pMa* strategy and this explained the lower *CN* (the difference between the main

260   combustion *HRR* peaks of the *pM* and *pMa* calibrations is greater in Fig. 7 than in Fig. 30). Finally, the ignition delay of

261   the main injected fuel in Fig. 30 is slightly longer, and the *HRR* peak attributed to the pilot combustion is higher for the

262   *pMa* schedule than for the *pM* one; both these results are physically consistent with the *CN* increase detected for the

263   *pMa* calibration [40].

264   In short, the after-injection only seems to have an indirect impact on the management of combustion noise. The addition

265   of the after shot to an injection train can produce relevant changes in the optimized *DoE* calibration. In particular, the

266   presence of the after injection can modify certain pilot injection parameters, such as pilot injection quantity and timing.

267   These parameters can influence the interaction between the pilot mixture field and the main injection, that is, the way

268   the main injection interferes with the ignition process of the pilot mixture and influences its combustion process, and

269   thus can significantly affect the combustion noise [40]. In general, in addition to the described interaction, hydraulic

270   interference between the pilot and main injections may also occur [41]. In fact, the different sets of pilot injection

271   masses and timings can generate different pressure values in the injector delivery chamber at the SOI_{main} instant, due to

272   the variability in the pressure wave dynamics. Therefore, the velocity at which the needle opens the nozzle during the

273   main energizing time can vary for the different calibrations and this can have an appreciable impact on the noise. In

274   general, the higher the needle velocity at the beginning of the main injection, the higher the combustion noise. This

275   hydraulic effect can be remarkable when pilot injections with lower DT than 500 μs are implemented, [6], but it is not

276   significant for the pilot-main DT considered in Fig. 30, (the enlargement in Fig. 30 shows smaller differences than 20%

277   in the injected flow-rate slope).

278   The *ppMa* calibration allows the *bsfc-NO_x* and the *CN-NO_X EGR* curves in Figs. 25 and 29 to be improved (cf. Table 7).

279   A slight benefit can also be observed in the management of the soot-NO_x trade-off (cf. Fig. 26). On the other hand, no

280   benefits can be observed for the quadruple injection with respect to the *HC-NO* (Fig. 27) or to the *CO-NO_X* (Fig. 28)

281   *EGR* trade-offs, compared to *pM* and *ppM* strategies.

282   Figures 31-33 report the burned gas temperature, the NO_x and the soot in-cylinder angular distributions for the baseline

283   calibration points of the four considered injection strategies. These diagrams, together with the *HRR* traces, complete

284   the in-cylinder numerical analysis. Even though *ppMa* features the highest T_b values (Fig. 31), the NO_x engine-out

285   emissions are minimized (Fig. 32). This behavior is probably due to the equivalence ratio distributions within the

286   cylinder.

287   Part of the fuel injected in the later-pilot injection burns during the main injection event in the *ppMa* baseline calibration

288   (cf. Fig. 30), and a larger amount of rich mixture (with $\phi \gtrsim 2$) results in the fuel spray of the main injection (the global O_2

289   concentration is also minimum for the *ppMa* case). As a consequence, the NO_x emissions diminish. For the same reason,

290   a great peak of soot can be seen in Fig. 33 for the *ppMa* case, although the energizing time of the main injection is

291   reduced, and the high T_b values and the appropriate timing of the after-injection, with respect to the main shot ($DT \approx 600$

292   μs), promote a greater oxidation of the soot generated during the main combustion. The *pM* baseline calibration shows

293   lower interference between pilot combustion and the main injection and employs the lowest X_{EGR} value. As a result, a

294   soot level minimum can be found at the engine exhaust (cf. Fig. 33). On the other hand, the high T_b values encountered

295   during diffusive combustion could explain the great increase in the NO_x over the $370° \ CA < \theta < 390° \ CA$ range for this

296   strategy. Furthermore, a significant production of NO_x also occurs for the *pM* strategy during the diffusive portion of

297   pilot-injected-fuel combustion, i.e., over the $360° \ CA < \theta < 365° \ CA$ range.

298   In the case of the *ppM* calibration, the higher rail pressure nominal value, i.e. $p_{rail} \approx 750$ bar instead of $p_{nom} \approx 620$ bar,

299   which is applied to all the other strategies at 1500x5, is responsible for the relatively high NO_x engine-out emissions that

300   can be observed in Fig. 32.

301   As far as the pilot injection is concerned, the highest temperatures of the unburned gases (cf. Fig. 31 for $\theta < 350°$ *CA*),

302   the reduced ignition delay of the fuel injected in the earlier pilot shot, and the major interference between the

303   combustion event pertaining to the earlier pilot injection and the fuel injected in the later pilot shot, are the reasons for

304   the augmented soot production over the $350°$ *CA* $< \theta < 365°$ *CA* interval in the *ppMa* case (cf. also Table 7).

305   The less steep pattern of the *HRR* curve for the *ppMa* calibration is the reason for the general lower combustion noise

306   level in Fig. 29. This *HRR* pattern is induced by the reduced entity of the premixed combustion, as a consequence of the

307   more pronounced interaction between the oxidation of the fuel, which is injected in the later pilot injection shot, and the

308   main injection.

309   # 6   CONCLUSIONS.

310   Multiple injection strategies featuring an after shot have been compared with pilot-main and pilot-pilot-main injection

311   strategies in a low-compression ratio Euro 5 diesel engine, in order to evaluate the possible benefits in engine-out

312   emissions, combustion noise and fuel consumption, at medium to high loads and at low to medium speeds.

313   All the triple and the quadruple injection strategies considered in this work have been optimized by means of a *DoE*

314   procedure: this aspect is relevant because it allows the effective benefits of the after injection to be assessed. *EGR* trade-

315   offs have been carried out around the baseline calibration points obtained from the *DoE* and around the *pM* injection

316   calibration. The latter represented the state-of-the-art double injection calibration of the considered engine technology.

317   Experimental tests have been conducted in a dynamometer cell and different steady-state key-points, which were

318   representative of the medium-high part load zone of the *NEDC* for a passenger car engine application, have been

319   considered. The experimental analysis has been supported by numerical results, which were derived from the

320   application of diagnostic combustion models, on the basis of the measured trace of the in-cylinder pressure time history.

321   The main outcomes concerning the effects of the after injection on pilot-main injection strategies with postponed main

322   injection timings are reported synthetically hereafter.

323   •   At medium to high loads and medium speeds, *DoE* optimized calibrations featuring after-injections with delayed

324   timings (10-15° *CA ATDC*) can improve engine-out NO_x emissions, compared to the *pM* baseline calibration, because

325   the after-injections take place at low in-cylinder pressures and gas temperatures. However, since the applied DT_{Aft}

326   values are relatively large, soot emissions grow and *bsfc* is slightly higher than in the case of the *pM* baseline

calibration. Furthermore, *CO* engine-out emissions tend to become worse for the *pMa* baseline calibration, due to the reduced temperatures of the after combustion.

- The soot-NO_x, *bsfc*-NO_x and *CO*-NO_x trade-offs of the engine calibration that employs the after injection do not change significantly, compared to those referring to a *PCCI* late strategy featuring a pilot-main injection schedule. Furthermore, the addition of the after-injections does not show any clear effect on the *HC*-NO_x trade-off, which can either improve or become worse, depending on the considered *bmep* and *n* values. However, the *HC* engine-out emissions are not a concern at medium speed and medium to high loads, which represent the typical working conditions of the after injection strategy.

- After-injection only seems to have only an indirect impact in the management of combustion noise. The addition of the after-shot to an injection train can produce relevant changes in a *DoE* optimized calibration. In particular, the presence of an after-injection can modify certain pilot injection parameters, such as the pilot injection quantities and timings. These parameters can influence the interaction between the pilot mixture field and the main injection, i.e., the way the main injection interferes with the ignition process of the pilot mixture and influences its combustion process. All this can have a significant effect on combustion noise. As proof of the complex correlation between the after-shot and combustion noise, a comparison between the *pM* and *pMa* experimental data has shown that, for the *pMa* calibration, the *CN* generally improves by 2 *dB* at *bmep*=5 bar and *n*=2000 rpm, but generally deteriorates by 1 dB at *bmep*=5 bar, *n*=1500 rpm and at *bmep*=12 bar, *n*=2750 rpm.

- The application of *ppMa* injection schedules at medium load and speed leads to improvements in the soot-NO_x, *bsfc*-NO_x trade-offs, compared to the *pM* and *ppM* strategies. Furthermore, *CN* reduces significantly, while the *CO*-NO_x trade-offs do not become worse. The presence of four injection shots leads to an increased flexibility in the management of the different constraints and in particular in the design of the best interaction between the pilot injection combustions and the main injection. A combination of *ppMa* strategies and high *EGR* rates is therefore recommended in low-compression ratio engines featuring delayed main injection timing.

7   NOMENCLATURE.

bmep   brake mean effective pressure

bsfc   brake specific fuel consumption

CA   crankshaft angle degree

CN   combustion noise

DOC   diesel oxygen catalyst

DoE   design of experiments

357	*DT*	dwell time
358	*ECU*	electronic control unit
359	*EGR*	exhaust gas recirculation
360	*HC*	unburned hydrocarbons
361	*HRR*	heat release rate
362	m_a	fresh air mass per stroke and per cylinder
363	$\dot{m}_a$	fresh air mass flow-rate
364	$\dot{m}_{EGR}$	exhaust gas recirculation mass flow-rate
365	*MFB50*	angle at which 50% of the combustion mixture has burned
366	*n*	engine speed
367	NO_x	nitrogen oxides
368	$O_{2\ int}$	oxygen volume concentration
369	p_{Boost}	boost pressure
370	p_{int}	pressure in the intake manifold
371	p_{cyl}	in-cylinder pressure
372	p_{rail}	nominal rail pressure level
373	*PCCI*	premixed charge compression ignition
374	*PM*	particulate matter
375	*q*	injected quantity (volume)
376	*TDC*	top dead center
377	*SOI*	electrical start of the injection
378	*Sw*	swirl actuator position
379	T_b	burned gas temperature
380	*TDC*	top dead center
381	X_{EGR}	mass fraction of exhaust gas recirculation
382	ϕ	equivalence ratio
383	λ	relative air-to-fuel ratio
384	θ	crankshaft angle in the simulations
385	***Subscripts***	
386	*Main*	main injection

387   *Pil1*   pilot 1 injection

388   *Pil2*   pilot 2 injection

389   *Aft*   after injection

390 **8   REFERENCES.**

391 [1] Mohan, B., Yang, W., and Chou, S. K., 2013, "Fuel injection strategies for performance improvement

392 and emissions reduction in compression ignition engines — A review", *Renewable and Sustainable Energy*

393 *Reviews*, vol. 28, pp. 664-676.

394 [2] Fang, Q., Fang, J., Zhuang, J., and Huang, Z., 2012, "Influences of pilot injection and exhaust gas

395 recirculation (*EGR*) on combustion and emissions in a HCCI-DI combustion engine", *Applied Thermal*

396 *Engineering*, vol. 48, pp. 97-104.

397 [3] Suh H.K., 2011, "Investigations of multiple injection strategies for the improvement of combustion and

398 exhaust emissions characteristics in a low compression ratio (CR) engine", *Applied Energy* 88 pp. 5013–

399 5019. doi:10.1016/j.apenergy.2011.06.048.

400 [4] Zheng M., Kumar R., 2009, "Implementation of multiple-pulse injection strategies to enhance the

401 homogeneity for simultaneous low-NOx and -soot diesel combustion". *International Journal of Thermal*

402 *Sciences* 48 pp. 1829–1841. doi:10.1016/j.ijthermalsci.2009.02.009.

403 [5] Kremer, F., Schaub, J., Steffens, C., and Kolbech, A., 2012"Optimizing the noise of future passenger car

404 diesel engines", MTZ, vol. 74, pp. 50-55.

405 [6] Ferrari, A., Mittica, A., and Spessa, E., 2013, "Benefits of hydraulic layout over driving system in piezo-

406 injectors and proposal of a new-concept CR injector with an integrated Minirail", *Apply Energy*, vol. 103, pp.

407 243-255.

408 [7] Ferrari, A., Paolicelli, F., and Pizzo, P., 2015, "The new-generation of solenoid injectors equipped with

409 pressure-balanced pilot valves for energy saving and dynamic response improvement"; *Applied Energy*, 151,

410 pp. 367-376.

411   [8] d'Ambrosio, S., and Ferrari, A., 2014, "Potential of double pilot injection strategies optimized with a

412   design of experiments procedure in the improvement of diesel engine emissions and performance",

413   submitted to *Applied Energy*.

414   [9] Helmantel, J., Somhorst, J., and Denbratt, I., 2003, "Visualization of the effects of post injection and

415   swirl on the combustion process of a passenger car Common Rail DI diesel engine", ICES2003-622,

416   Proceeedings of the ASME conference, Salzbury.

417   [10] Chen, S. K., 2000, "Simultaneous reduction of NO_x and particulate emissions by using multiple

418   injections in a small engine", SAE Paper No.° 2000-01-3084.

419   [11] Surushima, T., Zhang, L., and Ishii, Y., 1999, "A study of unburned HC emission in small DI diesel

420   engines", SAE Paper No. 1999-01-0512.

421   [12] Dronniou, N., Lejeune, M., Balloul, I., and Higelin, P., 2005, "Combination of High EGR Rates and

422   Multiple Injection Strategies to Reduce Pollutant Emissions," SAE Paper No. 2005-01-3726, 2005.

423   [13] Zheng, Z., Lang, Y., Liu, H., Zhu, Y., Zhong, X., and Yao, M., 2015, "Effect of two-stage injection on

424   combustion and emissions under high EGR rate on a diesel engine by fueling blends of diesel/gasoline,

425   diesel/n-butanol, diesel/gasoline/n-butanol and pure diesel", *Energy Conversion and Management*, vol. 90,

426   pp. 1-11.

427   [14] Walker, L.C., et al., 2011, "Method and system for reducing turbo lag in an engine", US Patent

428   Application 11/464.888 (Navistar).

429   [15] Parks, J., Huff, S., Kass, M., Sorey, J., 2007, "Characterization of in-cylinder techniques for thermal

430   management of diesel aftertreatment", SAE Paper No. 2007-01-3997.

431   [16] Guo, G., Warner, J., Cavataio, G., Dobson, D., Badillo, E., and Lambert, C., 2010, "The development of

432   advanced urea-SCR systems for Tier 2 Bin 5 and beyond diesel vehicles", SAE Paper No. 2010-01-1183.

433   [17] Desantes, J. M., Arrègle, J., Lopez, J. J., and Garcia, A., 2007, "A comprehensive study of diesel

434   combustion and emissions with post injection", SAE Paper No. 2007-01-0915.

435   [18] Dieselnet website, since 1997, "Engine & emission technology online", www.dieselnet.com.

436   [19] Han, Z., Uludogan, A., Hampson, G. J., Reitz, R. D., 1996, "Mechanism of soot and NO_x emission

437   reduction using multiple injection in a diesel engine", SAE Paper No. 960633.

438   [20] Mendez, S., and Thirouard, S., 2008, "Using Multiple Injection Strategies in Diesel Combustion:

439   Potential to Improve Emissions, Noise and Fuel Economy Trade-off in Low *CR* engines", SAE *Int. J. Fuels*

440   *Lubr.*, Vol. 1, Issue 1, pp. 662-674.

441   [21] Yun, H. H., Sellnau, M., Milovanovic, N., and Zuelch, S., 2008, "Development of premixed low-

442   temperature diesel combustion in a HSDI engine", SAE Paper No. 2008-01-0639.

443   [22] Park, C., Kook, S., and Bae, C., 2004, "Effects of multiple injections in a HSDI diesel engine equipped

444   with Common Rail injection system", SAE Paper No. 2004-01-0127.

445   [23] Arregle, J., Pastor, J. V., Lopez, J. J., and Garcia, A., 2008, "Insights on post injection-associated soot

446   emissions in direct injection strategies", *Combustion and Flame*, 154, pp. 448-461.

447   [24] Bobba, M., and Musculus, M., 2010 "Effects of post injections on in-cylinder and exhaust soot for low-

448   temperature combustion in a heavy-duty diesel engine", *SAE Int. J. Engines*, Vol. 3, issue 1, p. 497.

449   [25] Ojeda, W.D., Zoldak, P., Espinosa, R., and Kumar, R., 2009, "Development of a Fuel Injection Strategy

450   for Partially Premixed Compression Ignition Combustion," *SAE Int. J. Engines* 2(1):1473-1488.

451   [26] Thurnheer T., Edenhauser D., Soltic P., Schreiber D., Kirchen P., and Sankowski A., 2011,

452   "Experimental investigation on different injection strategies in a heavy-duty diesel engine: Emissions and

453   loss analysis", *Energy Conversion and Management*, 52, pp. 457–467.

454   [27] Lee, J. W., Choi, H., Hong, K., Lee, S., Yu, S., Choi, S.M., and Min, K.D., 2013, "Comparison of the

455   effects of multiple injection strategy on the emissions between moderate and heavy EGR rate conditions: part

456   2-post injections", *Journal of Mechanical Science and Technology*, 27(7), pp. 2217-2223.

457   [28] Helmantel, A., and Golovitchev, 2009, "Injection strategy optimization for a light duty DI diesel engine

458   in medium load conditions with high EGR rates", SAE Paper No. 2009-01-1441.

459 [29] Lee, J. W., Choi, H., Lee, S., Shin, S., Choi, S. M., Song, H., and Min, K. D., 2012, "Emission reduction

460 by close post injection strategy with modified nozzle and piston bowl geometry at diesel combustion with

461 heavy *EGR* rate", SAE Paper No. 2012-01-0681.

462 [30] Badami, M., Mallamo, F, and Millo, F., 2003, "Experimental investigation on the effect of multiple

463 injection strategies on emissions, noise and brake specific fuel consumption of an automotive direct injection

464 common-rail diesel engine", *International journal of engine research* 4(4), pp. 299-314.

465 [31] Badami, M., Mallamo, F, and Millo, F., 2002, "Analysis of multiple injection strategies for the

466 reduction of emissions, noise and bsfc of DI CR small displacement non-road diesel engine", SAE Paper

467 No. 2002-01-2672.

468 [32] Zheng Z., Yue L., Liu H., Zhu Y., Zhong X., and Yao M., 2015, "Effect of two-stage injection on

469 combustion and emissions under high EGR rate on a diesel engine by fueling blends of diesel/gasoline,

470 diesel/n-butanol, diesel/gasoline/n-butanol and pure diesel", *Energy Conversion and Management*, 90, pp. 1-

471 15.

472 [33] Finesso, R., and Spessa, E, 2014, "A real time zero-dimensional diagnostic model for the calculation of

473 in-cylinder temperatures, HRR and nitrogen oxides in diesel engines. *Energy Conversion and Management*

474 79 498–510. http://dx.doi.org/10.1016/j.enconman.2013.12.045.

475 [34] Akihama, K., Takatori, Y., Inagaki, K., Sakaki, S., and Dean, A. M., 2001, "Mechanism of smokeless

476 rich diesel combustion by reducing temperature", SAE Paper No. 2001-01-0655.

477 [35] Mohan, B., Yang, W., and Chlu, S. K., 2013, "Fuel injection strategies for performance improvement

478 and emission reduction in compression ignition engines - A review", *Renewable and Sustainable Energy*

479 *Reviews*, 28, pp. 664-676.

480 [36] Lee, J. W., Choi, S. M., Shin, S. H., Choi, M., and Min, K. D., 2012, "Experimental analysis of

481 emission reduction by the split injection strategy using close post injection with a double-row nozzle in

482 heavy EGR conditions", *Journal of Mechanical Science and Technology*, 26(4), pp. 1-10.

483 [37] Zhuang J, Qiao X, Bai J, Hu Z, 2014, "Effect of injection-strategy on combustion, performance and

484 emission characteristics in a DI-diesel engine fueled with diesel from direct coal liquefaction", *Fuel* 121 pp.

485 141–148. http://dx.doi.org/10.1016/j.fuel.2013.12.032.

486 [38] Gan S, Ng HK, Pang KM, 2011, "Homogeneous charge compression ignition (HCCI) combustion:

487 implementation and effects on pollutants in direct injection diesel engines". *Applied Energy*;88(3):559–567.

488 [39] Priede, T., 1979, "Problems and Developments in Automotive Engine Noise Research," SAE Technical

489 Paper No. 790205.

490 [40] Busch, S., Zha, K., and Miles, P. C., 2014, "Investigations of closely coupled pilot and main injections

491 as a mean to reduce combustion noise", Thiesel Conference, September 9th-12th, Valencia, Spain.

492 [41] Herfatmanesh M.R,. Lu P., Attar M.A., and Zhao H., 2013, "Experimental investigation into the effects

493 of two-stage injection on fuel injection quantity, combustion and emissions in a high-speed optical common

494 rail diesel engine", *Fuel* 109 pp. 137–147. http://dx.doi.org/10.1016/j.fuel.2013.01.013.

495 [42] Baratta M., Catania A.E., Ferrari A., Finesso R. and Spessa E., 2011, "Premixed-Diffusive Multizone

496 Model for Combustion Diagnostics in Conventional and PCCI Diesel Engines", *ASME Trans. Journal of*

497 *Engineering for Gas Turbines and Power*, vol. 133 n. 10, Art. No. 102801, pp. 1-13.

Engine type	2.0L Euro 5
Displacement	1956 cm^3
Bore × stroke	83.0 mm × 90.4 mm
Compression ratio	16.3
Valves per cylinder	4
Turbocharger	Twin-stage with valve actuators and WG
Fuel injection system	CR 2000 bar piezoelectric indirect acting injectors
Specific power and torque	71 kW/l – 205 Nm/l
EGR system type	Short-route cooled EGR
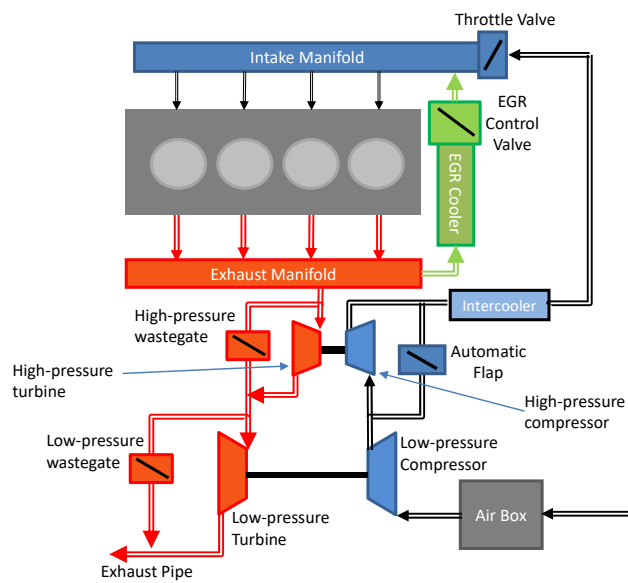
Table 1: Main specifications of the reference engine.

Quantity	Levels							Optimization
SOI_{Main} [°CA bTDC]		−3	−1	1				1
m_a [mm^3/(stk·cyl)]	360	380	390	400	420			384
Sw [%]		30	40	50				30
p_{Rail}[bar]	750	850	950	1050	1150			750
q_{Pil} [mm^3/(stk·cyl)]	0.8	1.1	1.4	1.7	2			1.42
DT_{Pil} [µs]	600	850	1100	1350	1600			600
q_{Aft} [mm^3/(stk·cyl)]	1	1.5	2	2.5	3			1
DT_{Aft} [µs]	600	933	1267	1600	1933	2267	2600	1082

Table 2: Levels considered for the variation list and optimized values of the inputs for the pMa injection strategy at 2000×5.

499

Quantity	Levels	Optimization
SOI_{Main} [°CA bTDC]	4 5 6 7 8	6.19
m_a [mm^3/(stk·cyl)]	680 690 700 710 720	720
Sw [%]	10 27.5 45	25
p_{Rail} [bar]	1500 1575 1650 1725 1800	1504.3
q_{Pil} [mm^3/(stk·cyl)]	0.7 1 1.3	0.7
DT_{Pil} [µs]	800 1000 1200 1400 1600	1600
q_{Aft} [mm^3/(stk·cyl)]	0.7 1.25 1.8 2.35 2.9 3.45 4	0.7
DT_{Aft} [µs]	800 950 1100 1250 1400	1203
p_{Boost} [mbar]	2200 2300 2400 2500 2600	2563

Table 3: Levels considered for the variation list and optimized values of the inputs for the pMa injection strategy at 2750×12.

500

501

Quantity	Levels	Optimal
SOI_{Main} [°CA bTDC]	−4 −2 0	0
m_a [mm^3/(stk·cyl)]	340 357.5 392.5 410	358.1
Sw [%]	30 40 50	44
p_{Rail}[bar]	600 700 800 900 1000	620.1
q_{Pil1} [mm^3/(stk·cyl)]	0.8 1.1 1.4 1.7 2	1
DT_{Pil1} [µs]	600 850 1100 1350 1600	905
q_{Pil2} [mm^3/(stk·cyl)]	0.8 1.15 1.5	0.8
DT_{Pil2} [µs]	600 850 1100 1350 1600	614
q_{Aft} [mm^3/(stk·cyl)]	0.8 1.35 1.9 2.45 3	0.8
DT_{Aft} [µs]	600 1000 1400 1800 2200 2600 3300	684

Table 4: Levels considered for the variation list and optimized values of the inputs for the ppMa injection strategy at 1500×5.

502

Strategy	NOx [g/kWh]	HC [g/kWh]	CO [g/kWh]	Soot [g/kWh]	bsfc [g/kWh]	CN [dBA]
pM	0.99	0.3	1.9	0.3	247	86.5
pMa	min	≤0.5	≤3	≤0.7	≤250	≤86.5

Table 5: Reference values of the reference *pM* calibration baseline point and constraints for the optimization of the *pMa* injection strategy at 2000×5.

503

Strategy	NOx [g/kWh]	HC [g/kWh]	CO [g/kWh]	Soot [g/kWh]	bsfc [g/kWh]	CN [dBA]
pM	1.7	0.09	0.9	0.17	223	87.1
pMa	min	≤0.1	≤0.9	≤0.3	≤230	≤87.1

Table 6: Reference values of the reference pM calibration baseline point and constraints for the optimization of the *pMa* injection strategy at 2750×12.

504

Strategy	NOx [g/kWh]	HC [g/kWh]	CO [g/kWh]	Soot [g/kWh]	bsfc [g/kWh]	CN [dBA]
pM	0.89	0.33	1.8	0.17	235	80.5
ppMa	min	≤0.33	≤2	≤0.4	≤235	≤79

Table 7: Reference values of the reference *pM* calibration baseline point and constraints for the optimization of the *ppMa* injection strategy at 1500×5.

505
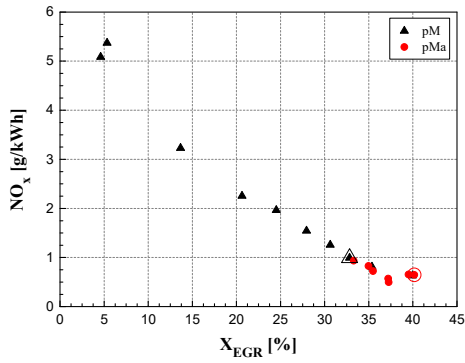
Figure 1. *NO$_X$-X$_{EGR}$ curve for the *pM* and *pMa* strategies (*bmep*=5 bar, *n*=2000 rpm).*
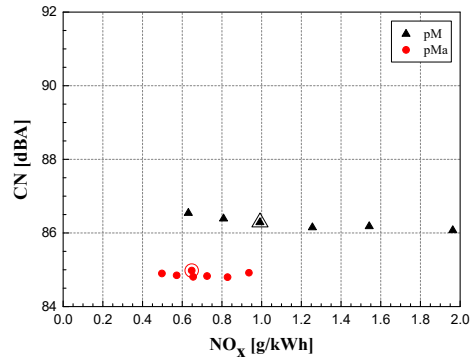
Figure 2. *CN-NO$_X$ trade-off for the *pM* and *pMa* strategies (*bmep*=5 bar, *n*=2000 rpm).*
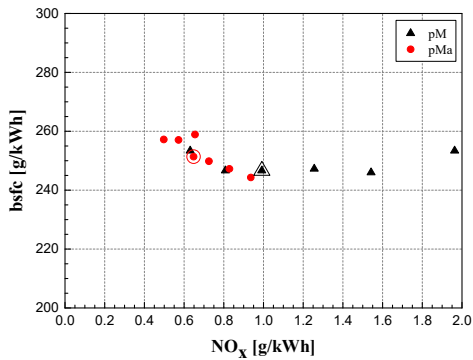
Figure 3. *bsfc-NO$_X$ trade-off for the *pM* and *pMa* strategies (*bmep*=5 bar, *n*=2000 rpm).*
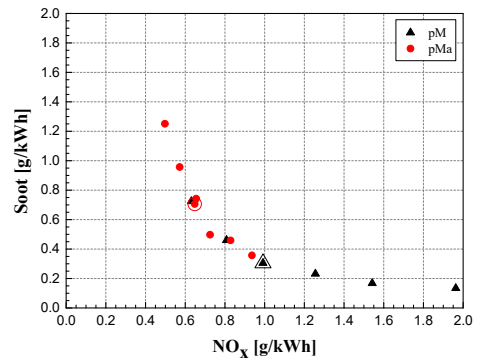
Figure 4. CO-*NO$_X$* trade-off for the *pM* and *pMa* strategies (*bmep*=5 bar, *n*=2000 rpm).
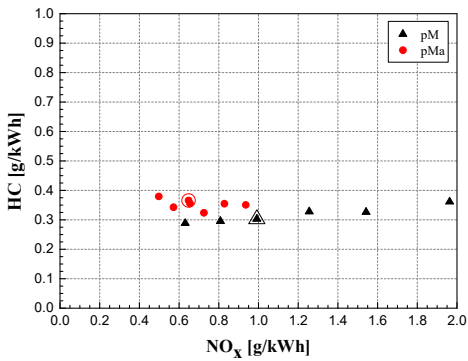
Figure 5. *HC-NO$_X$* trade-off for the *pM* and *pMa* strategies (*bmep*=5 bar, *n*=2000 rpm).
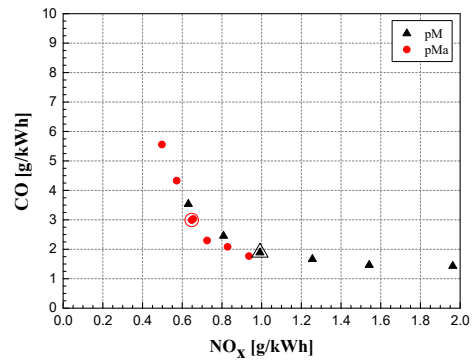
Figure 6. CO-*NO$_X$* trade-off for the *pM* and *pMa* strategies (*bmep*=5 bar, *n*=2000 rpm).
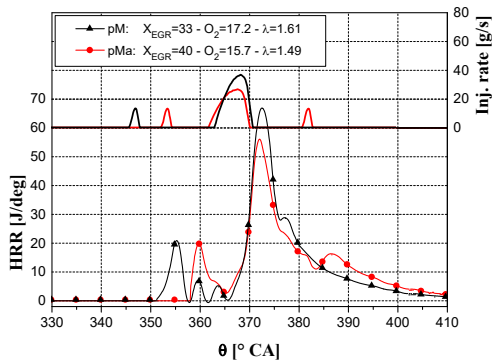
Figure 7. *HRR* versus θ distribution for the *pM* and *pMa* strategies (*bmep*=5 bar, *n*=2000 rpm).
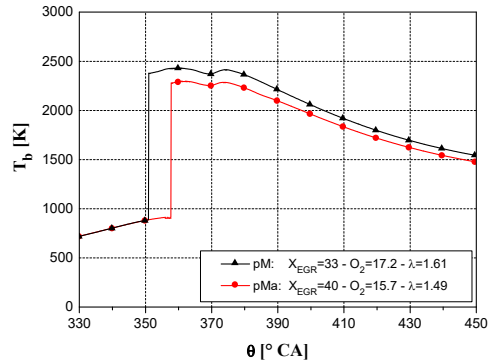
Figure 8. *T$_b$* versus θ distribution for the *pM* and *pMa* strategies (*bmep*=5 bar, *n*=2000 rpm).
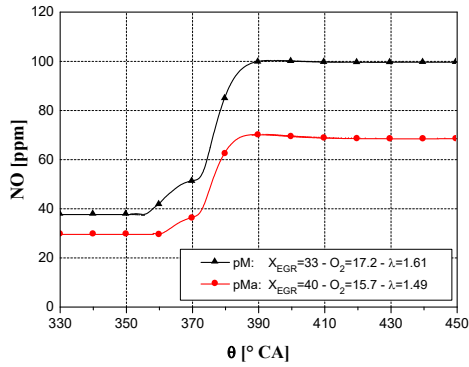
Figure 9. *NO* versus θ distribution for the *pM* and *pMa* strategies (*bmep*=5 bar, *n*=2000 rpm).
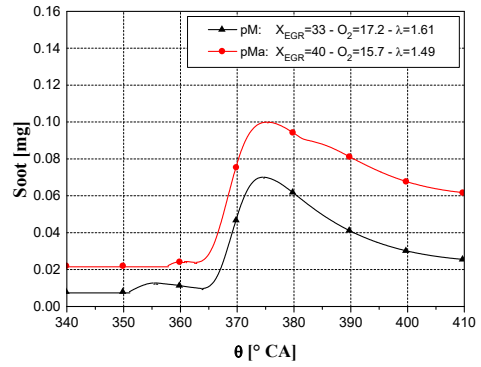
Figure 10. *PM* versus θ distribution for the *pM* and *pMa* strategies (*bmep*=5 bar, *n*=2000 rpm).
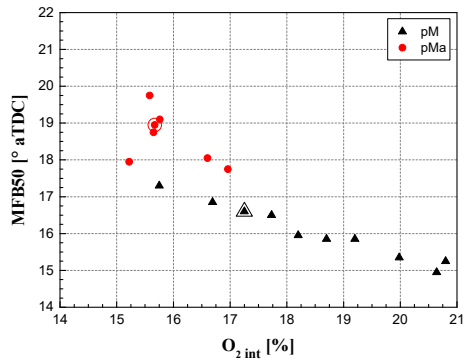
Figure 11. *MFB50* as a function of X_{EGR} for the *pM* and *pMa* strategies (*bmep*=5 bar, *n*=2000 rpm).
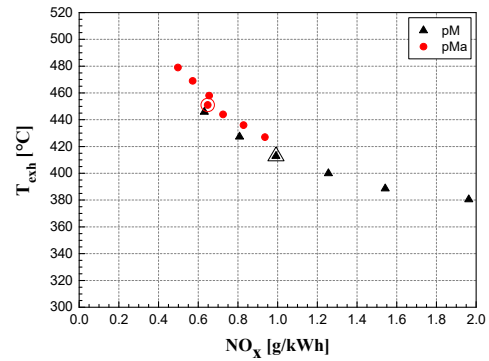
Figure 12. T_{exh} as a function of X_{EGR} for the *pM* and *pMa* strategies (*bmep*=5 bar, *n*=2000 rpm).
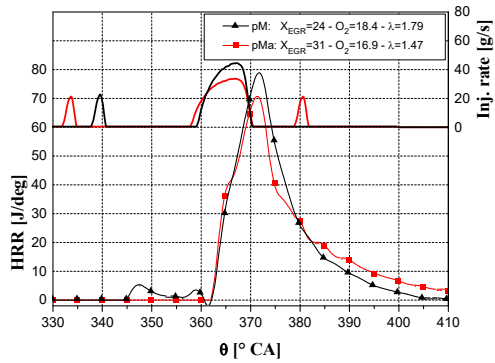
Figure 13. *HRR* versus θ distribution for the *pM* and *pMa* strategies (*bmep*=8 bar, *n*=2500 rpm).
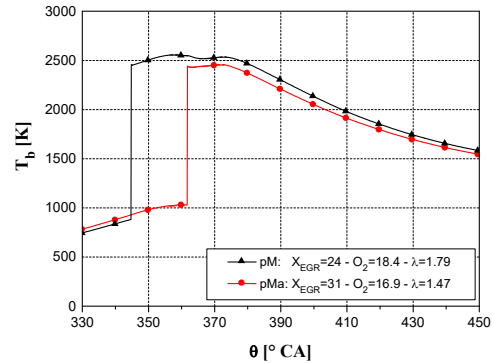
Figure 14. T_b versus θ distribution for the *pM* and *pMa* strategies (*bmep*=8 bar, *n*=2500 rpm).
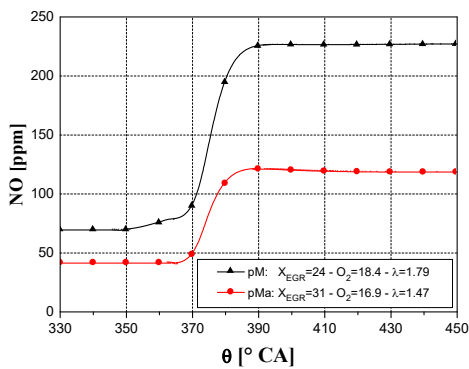
Figure 15. NO_x versus θ distribution for the *pM* and *pMa* strategies (*bmep*=8 bar, *n*=2500 rpm).
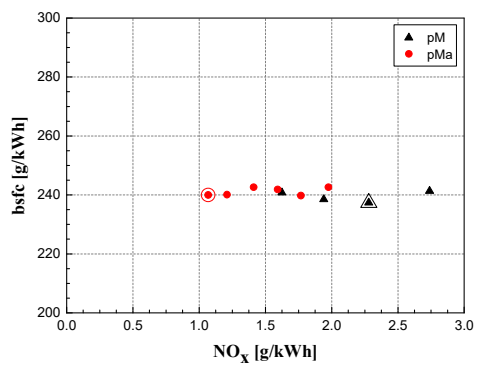
Figure 16. *bsfc-NO_x* trade-off for the *pM* and *pMa* strategies (*bmep*=8 bar, *n*=2500 rpm).

507
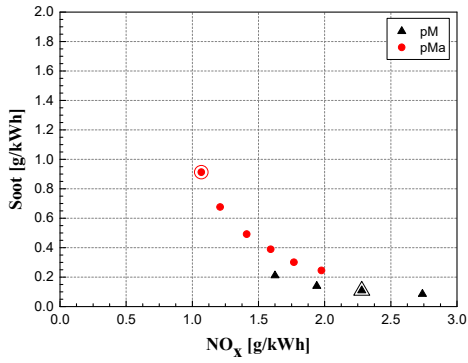
Figure 17. Soot-*NO$_X$* trade-off for the *pM* and *pMa* strategies (*bmep*=8 bar, *n*=2500 rpm).
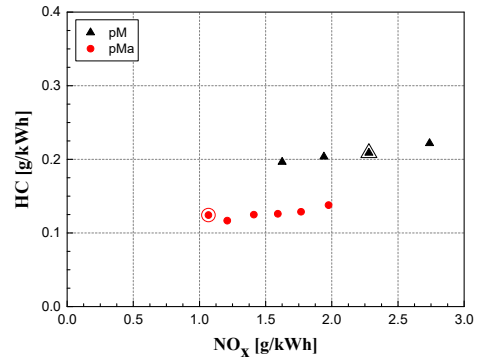
Figure 18. *HC-NO$_X$* curve for the *pM* and *pMa* strategies (*bmep*=8 bar, *n*=2500 rpm).
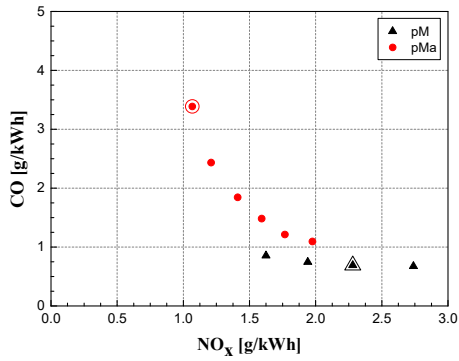
Figure 19. *CO-NO$_X$* trade-off for the *pM* and *pMa* strategies (*bmep*=8 bar, *n*=2500 rpm).
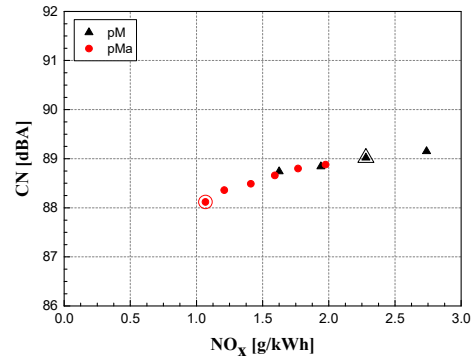
Figure 20. *CN-NO$_X$* curve for the *pM* and *pMa* strategies (*bmep*=8 bar, *n*=2500 rpm).
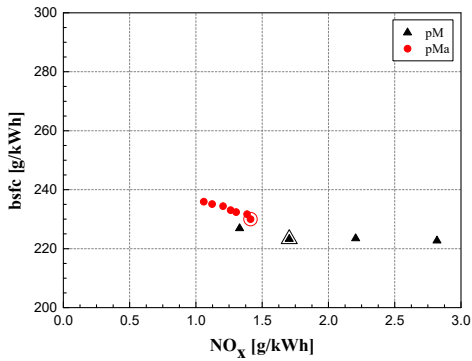
Figure 21. *bsfc-NO$_x$* trade-off for the *pM* and *pMa* strategies (*bmep*=12 bar, *n*=2750 rpm).
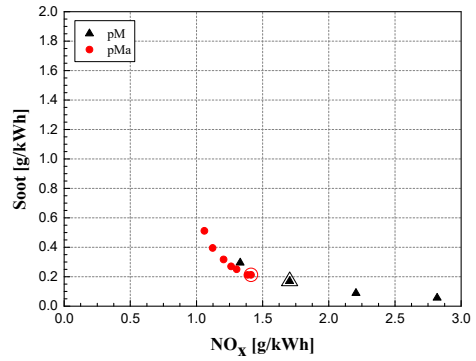
Figure 22. Soot-*NO$_X$* trade-off for the *pM* and *pMa* strategies (*bmep*=12 bar, *n*=2750 rpm).
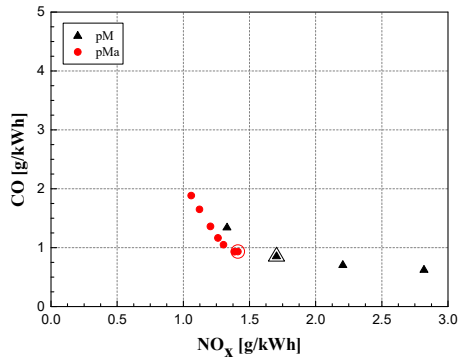
Figure 23. CO-*NO$_X$* trade-off for the *pM* and *pMa* strategies (*bmep*=12 bar, *n*=2750 rpm).
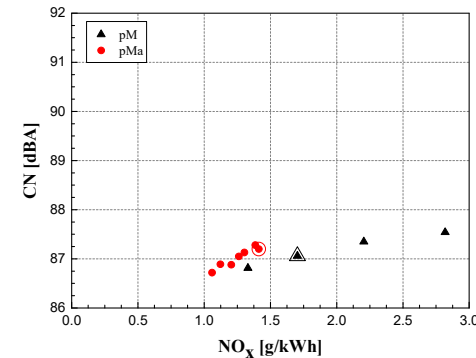
Figure 24. *CN-NO$_X$* curve for the *pM* and *pMa* strategies (*bmep*=12 bar, *n*=2750 rpm).
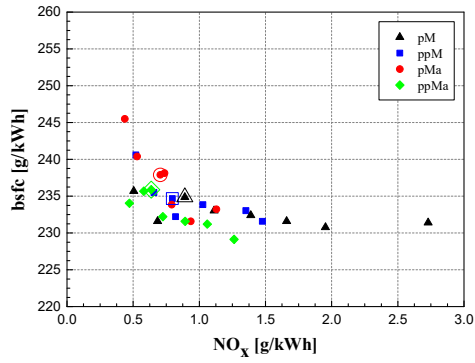
Figure 25. *bsfc-NO$_X$* trade-off for the *pM*, *ppM*, *pMa* and *ppMa* strategies (*bmep*=5 bar, *n*=1500 rpm).
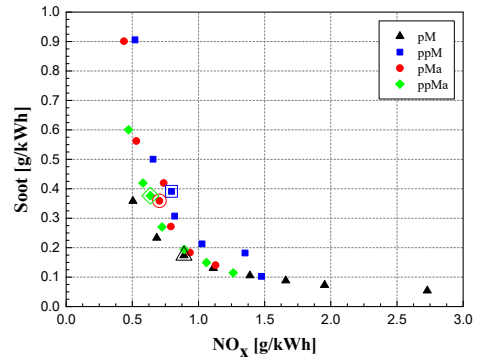
Figure 26. Soot-*NO$_X$* trade-off for the *pM*, *ppM*, *pMa* and *ppMa* strategies (*bmep*=5 bar, *n*=1500 rpm).
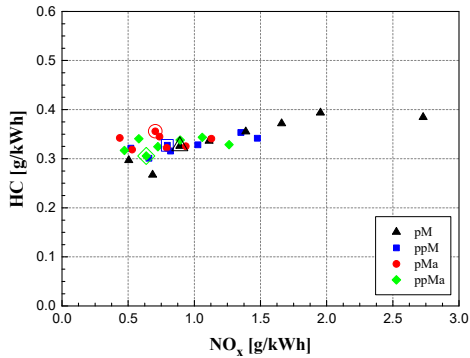
Figure 27. *HC-NO$_X$* trade-off for the *pM*, *ppM*, *pMa* and *ppMa* strategies (*bmep*=5 bar, *n*=1500 rpm).
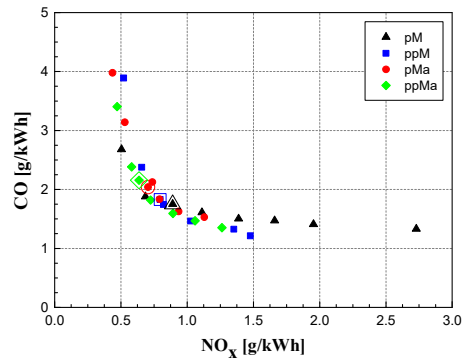
Figure 28. *CO-NO$_X$* trade-off for the *pM*, *ppM*, *pMa* and *ppMa* strategies (*bmep*=5 bar, *n*=1500 rpm).
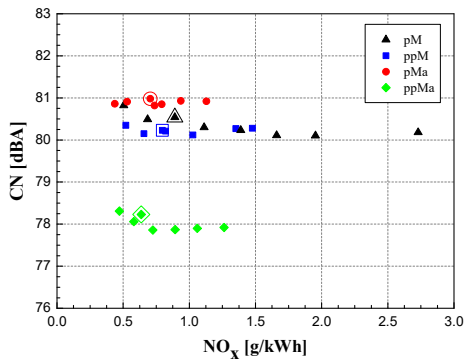
Figure 29. *CN-NO$_X$* curve for the *pM*, *ppM*, *pMa* and *ppMa* strategies (*bmep*=5 bar, *n*=1500 rpm).
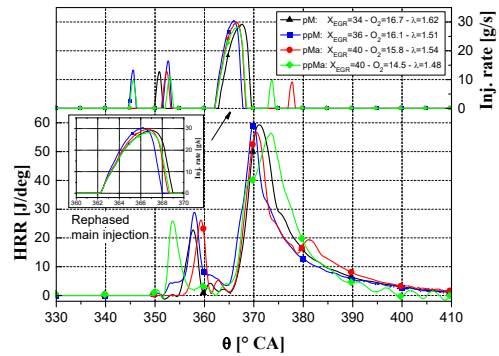
Figure 30. *HRR* versus θ distribution for the *pM*, *ppM*, *pMa* and *ppMa* strategies (*bmep*=5 bar, *n*=1500 rpm).
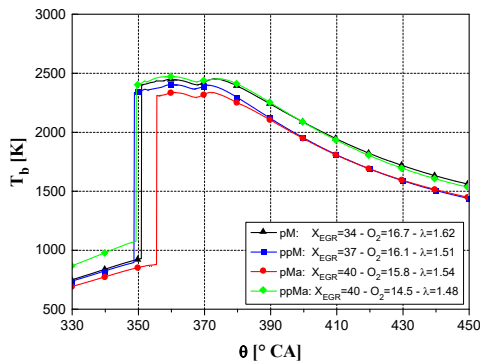
Figure 31. *T$_b$* versus θ distribution for the *pM*, *ppM*, *pMa* and *ppMa* strategies (*bmep*=5 bar, *n*=1500 rpm).
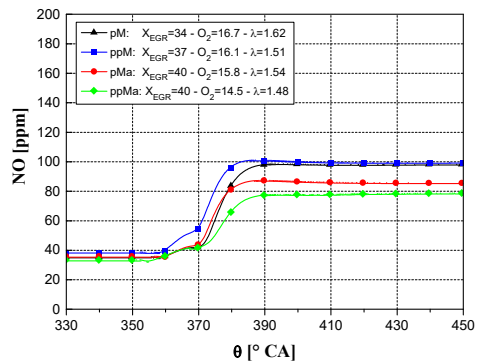
Figure 32. *NO$_x$* versus θ distribution for the *pM*, *ppM*, *pMa* and *ppMa* strategies (*bmep*=5 bar, *n*=1500 rpm).
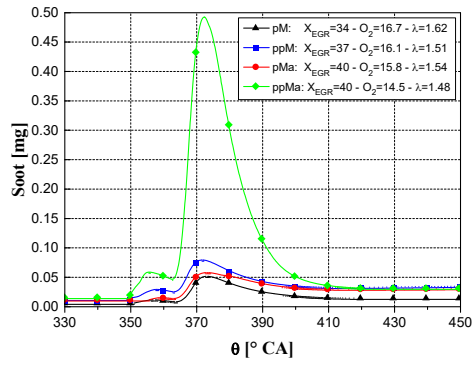
Figure 33. Soot versus θ distribution for the *pM*, *ppM*, *pMa* and *ppMa* strategies (*bmep*=5 bar, *n*=1500 rpm).

510